Chapitre 4:

Effets des contraintes épitaxiales dans $La_{2/3}Ca_{1/3}MnO_3$

4 Effets des contraintes épitaxiales dans les manganites

Des études théoriques et expérimentales effectuées sur les manganites ont montré que leurs propriétés magnétiques et de transport sont le résultat de la compétition entre le caractère itinérant de l'électron e_g du Mn^{+3}, régi par l'interaction de double échange, et les tendances de localisation dues à la forte interaction électron-réseau cristallin. Ces interactions sont en concurrence et certaines déformations cristallographiques favorisent l'une ou l'autre. Une compression uniforme peut être réalisée par une "pression chimique interne", qui consiste à induire une déformation isotrope du réseau cristallin par la substitution du cation A par une autre terre rare (RE) trivalente avec un rayon ionique différent. Dans ce cas, pour un niveau de dopage fixé, la substitution par des RE plus petites a comme résultat la réduction de la T_C et l'augmentation de la CMR [7, 8, 48]. L'origine proposée pour expliquer les effets de la pression interne sur la CMR est la variation de l'angle de la liaison Mn-O-Mn [118], qui contrôle l'interaction de double échange. Cependant, l'application d'une pression hydrostatique sur des manganites qui présentent la transition FM/PM a comme effet l'augmentation des interactions FM, la réduction de la résistivité à toute température et l'augmentation de la T_C (2.2 K/kbar)[45, 46, 119]. Les effets d'une pression hydrostatique externe ont été expliqués à partir de la réduction uniforme du volume, ce qui a comme effet l'augmentation de l'angle <Mn-O-Mn> et la réduction de d_{Mn-O} , augmentant ainsi l'interaction de DE [120]. Dans les oxydes à base de Ni ($RENiO_3$), les expériences de diffraction de neutrons sous pression hydrostatique externe ou interne donnent lieu à des résultats similaires [121].

Certaines déformations anisotropes ont été étudiées théoriquement [122] et prédisent qu'elles diminuent la T_C et modifient la CMR par l'augmentation de l'énergie Jahn-Teller qui induit la localisation des électrons. Une déformation biaxiale produit la diminution de T_C. Les auteurs déduisent une variation de 10% de T_C pour une contrainte biaxiale de 1% dans des systèmes comme les manganites à fort couplage électron-réseau. Récemment, une étude a rapporté l'effet d'une pression uniaxiale dans un monocristal de $Nd_{1/2}Sr_{1/2}MnO_3$. Les auteurs concluent que la pression uniaxiale augmente la température de l'ordre de charge et diminue T_C en accord avec les prédictions théoriques [47].

Dans ce chapitre, nous allons étudier l'effet de la contrainte épitaxiale dans les propriétés des couches de LCMO sur $SrTiO_3$(001).

4 Stress effects in manganites

Theoretical and experimental works performed on CMR manganites have shown that transport and magnetic properties of mixed valence manganites are based on the interplay between the Mn e_g electron itinerancy governed by the double exchange interaction and the localising effect of a strong electron–lattice coupling. These interactions compete and certain deformation of the lattice favours one or the other depending on the deformation . Uniform compression has been achieved by what has been called “internal chemical pressure”, which consist in isotropic deformation of the lattice induced by the substitution of the A cation by other trivalent rare earths with smaller or bigger radius. In this case, for a fixed doping level, the introduction of a smaller trivalent rare earth induces the reduction of T_C and as a consequence an increase of the CMR [7, 8, 48]. The effects of internal pressure on the CMR have been proposed to be mainly due to Mn-O-Mn bond angle variation [118], which tunes the double exchange interaction. However, the application of external hydrostatic pressure on manganites exhibiting the FM to PM transition tends to increase the intensity of FM interactions, reduces the resistivity at all temperatures and raises T_C (2.2K/kbar)[45, 46, 119]. External pressure effects have been explained to have their origin in the uniform volume reduction which tends to increase the <Mn-O-Mn> mean angle and to reduce d_{Mn-O} and thus to enhance the DE interaction [120]. In parent Ni oxides compounds ($RENiO_3$), neutron diffraction experiments under external hydrostatic pressure and internal pressure demonstrate similar results [121].

Another type of deformation are the anisotropic deformations. This kind of deformations has been theoretically studied [122] and the authors predict that they modify T_C and the CMR by increasing the Jahn-Teller splitting and thus the tendency of the electrons to localise. That means that biaxial deformation tends to decrease T_C. The authors deduced a 10% variation of T_C change under 1% of biaxial strain in strongly electron-lattice interacting systems as manganites. Recently, it has been reported a study on the effect of uniaxial pressure in $Nd_{1/2}Sr_{1/2}MnO_3$ single crystal. The authors concluded that uniaxial pressure tends to increase the charge ordering temperature while lowering T_C in agreement with Millis’s conclusions [47].

In the present study, we will focus on substrate strain induced effects in epitaxially grown manganite thin films of LCMO on $SrTiO_3$ substrates.

4.1 Epitaxial strain in $La_{2/3}Ca_{1/3}MnO_3$

As shown in section 3.1.1, the lattice parameter of $SrTiO_3$ (3.905Å) is closer to the lattice parameter of LCMO (3.855Å) than MgO (4.216Å). This better lattice match is compatible with real epitaxial growth. This 1% of mismatch will lead to strained films, at least until a critical thickness where relaxation process take place. We will demonstrate that films deposited on mismatched $SrTiO_3$ substrates exhibit differences in the transport features respect to unstrained single crystals of the same composition.

A series of LCMO films on $SrTiO_3$ with different thickness (thickness range 30nm-200nm) were prepared by pulsed laser deposition. All the samples were deposited using the same deposition conditions: substrate temperature of 760°C, using a UV(352nm) laser and a fluence of 3J/cm^2, in a background oxygen pressure of 300mTor and a cooling down performed at 5 deg/minute in 1bar of O_2. The rms roughness extracted from 1µm^2 AFM contact measurements is about 9Å, which revealed flat surfaces as shown in Fig. 4-1.

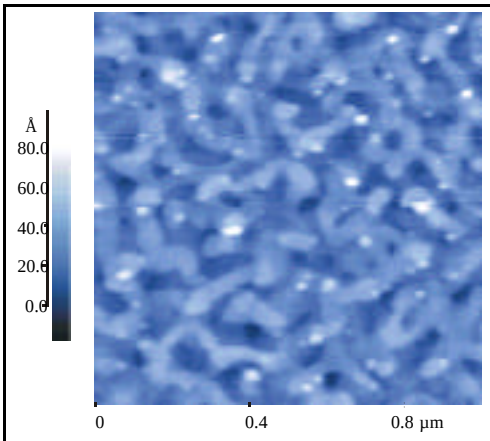

Fig. 4-1 *AFM contact picture of 1µm^2 surface displaying a flat surface in a 30nm LCMO film epitaxially grown on STO (rm :9Å) .*

From the inspection of the lattice parameters of bulk LCMO and STO, the grown films are expected to be under tensile stress in the in plane directions with $\varepsilon_{xx}=\varepsilon_{yy}$= 1.3%. The stress ε is defined as $\varepsilon_{xx}(\%) = \frac{a_{film} - a_{ref}}{a_{ref}}$ where a_{ref} is the reference lattice parameter. Considering a Poisson's ratio of 0.3 as given in [123] for $La_{2/3}Ba_{1/3}MnO_3$, we deduce an out of plane distortion $\varepsilon_{zz} = -\frac{2\nu}{(1-\nu)}\varepsilon_{xx} = -1.1\%$ which in terms of *c* lattice parameter would give *c*=3.813Å instead of the bulk value of 3.855Å. So a tetragonal structure with shortened out of place cell parameter and expanded in plane cell parameters is expected in the strained films on $SrTiO_3$.

From θ-2θ XRD measurements, we deduce that all LCMO films on STO substrate are (001) textured. In Fig. 4-2 is shown the evolution of the (003) peak with the film thickness.

In order to know the evolution of the in-plane cell parameters GID measurements have been also performed on the same film series. In Fig. 4-3 are shown the in plane, (*a*), and out of plane, (*c*), cell parameters. In plane cell parameter, for films thinner than 60nm, agrees with the STO cell

parameter. That suggests that films thinner than 60nm are completely strained. Thicker films display a relaxation of the in-plane and out-of-plane cell parameters, which is found closer to the bulk value.

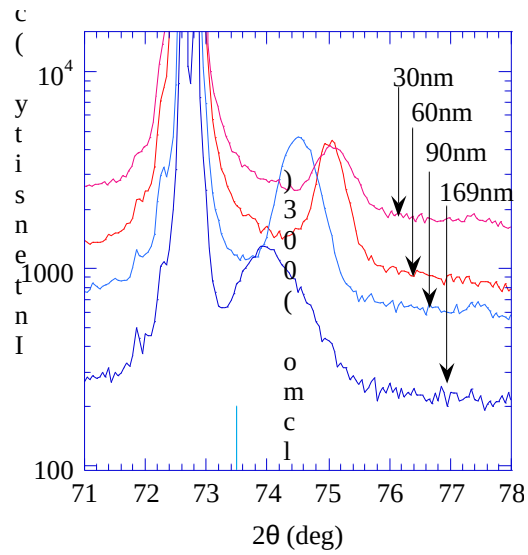

Fig. 4-2 *X-Rays θ-2θ diffraction patterns for LCMO/STO films of different film thickness.*

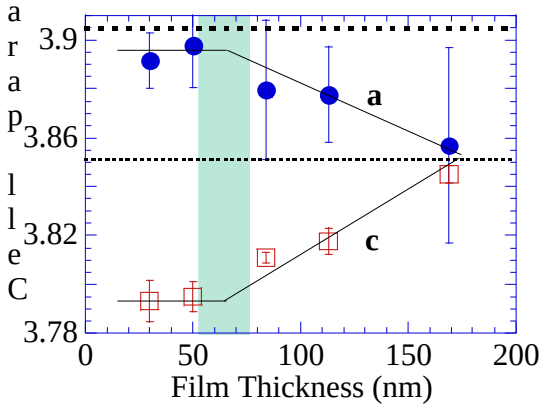

Fig. 4-3 *In plane, a, and out of plane, c, cell parameters of the LCMO films on STO vs the film thickness. The thick dashed line corresponds to the STO cell parameter while the thinnest corresponds to the target cell parameter.*

The FWHM of the (00●) peaks increases with the film thickness as shown in Fig. 4-4. Considering the Laue-Scherrer formula and relating the size of the coherently diffracting crystallites with the thickness of the film, a decrease of the FWHM is expected when increasing the film thickness. The increase of the FWHM for larger thickness observed experimentally is then in contradiction with the expected behaviour. However, this unexpected evolution of the FWHM can be attributed to the existence of microstructural inhomogeneities, as for example a distribution of cell parameters.

The cell parameters attained by the thicker films correspond to the target's cell parameter (Fig. 4-3). Thinner films do not exhibit any difference in the stoichiometry as checked by standard techniques as RBS or EDX (Tab.5-1). EDX measurements show that the composition of the films are the same within 2% of error for thick and thin films. The oxygen content can not be checked out by RBS nor by EDX. One way to tune the oxygen content is the annealing in oxygen atmosphere. In this sense, the annealing procedure used in the film growth has been the same for all the films and has shown to be enough in thick films to give a correct T_C.

From the crystallographic measurements, we conclude that LCMO films deposited on STO substrates are fully strained up to a critical thickness of about 60nm. Above this thickness, the accumulated elastic energy is probably released through the creation of defects and dislocations. In agreement, this assumption there are HRTEM measurements performed by other authors[110, 124-126].

30nm Thick LCMO film on STO			90nm thick LCMO film on STO		
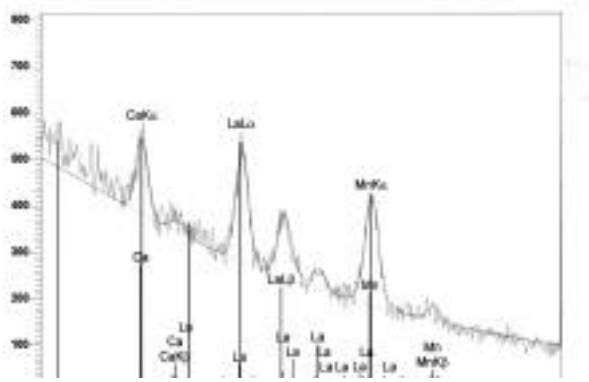			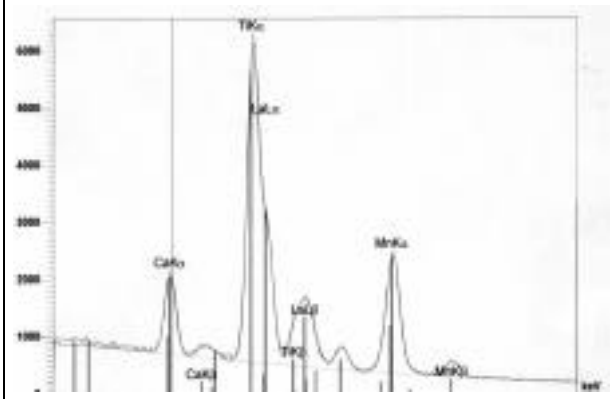		
Element	% Atomic	Composition	Element	% Atomic	Composition
La	34.37	0.68	La	35.45	0.69
Ca	15	0.30	Ca	13.58	0.27
Mn	50.63	1	Mn	50.97	1

Tab. 4-I *EDX measurements on a 30nm and 90nm thick LCMO films on STO substrate*

From our measurements, the critical film thickness corresponds to 60±10nm in contrast with the value of 20nm reported by Zandbergen et al. on the same system [127]. It is not unusual to obtain differences in the critical thickness due to the non equilibrium state of strained films, the different deposition techniques, and deposition temperatures and annealing used by the authors [128]. Other authors have reported fully strained 58nm thick LCMO films on STO substrates deposited by MBE [129]. And for very thick films (>650nm), macroscopic cracks appear as reported by Gommert et al.

A series of LCMO films on MgO(001) substrate with different thickness ranging from 15nm to 60nm, has also been prepared. Comparing the value of the out of plane cell parameter, for similar film thickness of LCMO on STO and on MgO substrates (Fig. 4-4), we conclude that because STO substrates allow real epitaxy because they match better the LCMO bulk cell parameters than MgO substrates, films on STO substrates are more strained up to thickness which are large compared to usual film thickness. The films on MgO have relaxed lattice parameter, similar to the bulk material. The lattice mismatch between LCMO and the MgO substrate is too large and thus it is impossible to match the substrate cell parameter.

HREM measurements performed by Gommert et al. on LCMO/STO films, agree with this idea and show that in the first 5 to 10nm of the LCMO film on STO the film grows epitaxially and nearly defect free. However, for LCMO films on MgO, the authors pointed out the existence of dislocations that compensate the lattice mismatch at the interface and then the film grows unstrained.

The observed existence of strain for thin films of LCMO on STO explains the anomalous behaviour of the FWHM (Fig. 4-4). There exist a distribution of cell parameters in the film and thus thicker films display larger FWHM.

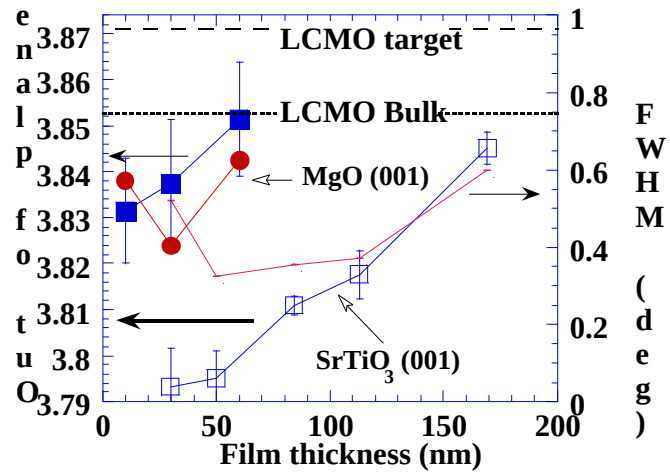

Fig. 4-4 *Evolution of de c cell parameter and the FWHM as a function of the film thickness for two series of LCMO films deposited on matched STO and non matched MgO substrates.*

The distribution of the cell parameters takes place in the in-plane and out-of-plane directions. GID measurements around the (110) and (200) directions for the 120nm thick film display a peak broadening when compared with the 30nm thin film (Fig. 4-5 and Fig. 4-6). The (200) peak of the STO substrate displays a FWHM= 0.1° while the 30nm LCMO/STO film displays FWHM=0.12° and it is very close to the substrate value. However, the value in the FWHM of the thicker film (120nm) is 0.36°, which is twice the value of the substrate.

In addition, the mosaicity of the thicker film is about 2° that contrast with the 0.3° of the thinner film (Fig. 4-5 and Fig. 4-6).

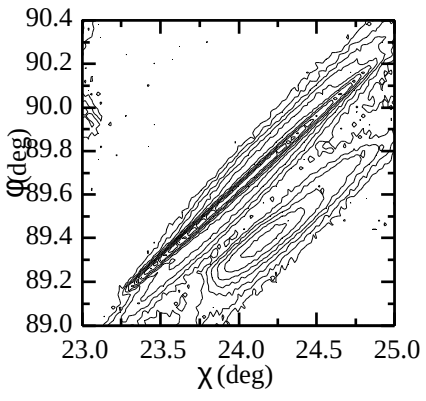

Fig. 4-5 *ϕ scans around the (200) in plane reflection for 112nm thick LCMO films on STO .*

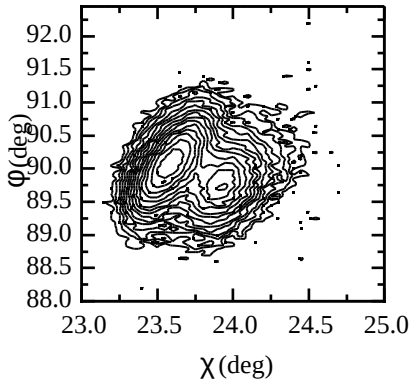

Fig. 4-6 *ϕ scans around the (200) in plane reflection for 30nm LCMO films on STO .*

Considering the experimental ε_{xx} and ε_{zz} values obtained in the present work (**Fig. 4-7**), we have estimated the value of the Poisson's ratio using $\varepsilon_{zz}/\varepsilon_{xx}= 2\nu/(1-\nu)$, which gives a value $\nu=0.39$,

quite similar to the values obtained for the parent compounds $La_{2/3}Sr_{1/3}MnO_3$ ν=0.42 and $La_{0.8}Ca_{0.2}MnO_3$, ν=0.38 [130].

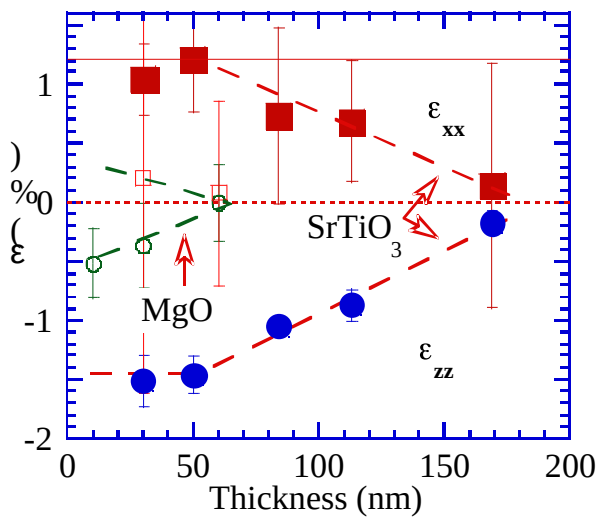

Fig. 4-7 *Stress vs film thickness for LCMO films deposited on STO and MgO. The continuous line at ε_{xx}= 1.2% is the calculated value for fully strained films on STO substrates*

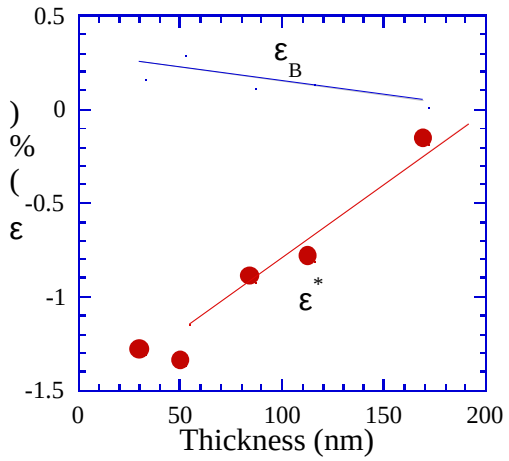

Fig. 4-8 *Evolution of the bulk (ε_B) and anisotropic strain (ε^*)with the film thickness*

Two of the parameters that permit to characterise the strain are: ε^* (biaxial strain) and ε_B (bulk strain) defined in Eq. 4-1. They permit to characterise the anisotropy and the volume of the unit cell respectively:

$$\varepsilon^* = \frac{1}{4}\left(2\varepsilon_{zz} - \varepsilon_{xx} - \varepsilon_{yy}\right)$$
$$\varepsilon_B = \frac{1}{3}\left(\varepsilon_{xx} + \varepsilon_{yy} + \varepsilon_{zz}\right) \qquad \textbf{Eq. 4-1}$$

An estimation of these parameters in LCMO films on STO substrates is shown in (Fig. 4-8). Bulk strain remains nearly constant with film thickness indicating that the volume of the unit cell is constant. However, the anisotropic strain is constant for film thickness below the critical film thickness for strain release, and diminishes for thicker films. Consequently, the crystallographic distortion of the LCMO structure induced by epitaxial growth is highly anisotropic but the unit cell volume is kept constant.

4.2 Modification of magnetotransport properties due to epitaxial strain

All the thin films of LCMO epitaxially grown on STO(001) in the thickness range between 30nm to 170nm do exhibit the FM-M to PM-I transition. However, in the literature, there exist a big dispersion of the value of the transition temperatures T_C for $La_{2/3}Ca_{1/3}MnO_3$ films depending on the substrate nature, deposition techniques and annealing.

Here we will show that films grown using the same procedure display a variety of T_C which are related to the strain induced by epitaxial growth. The observation of magnetic anisotropy for thinner films (section 4.3) permits to rule out the possibility of oxygen stoichiometry differences between the films.

In Fig. 4-9 are shown the thermal evolution of the spontaneous magnetisation, obtained from isothermal M(H) curves of LCMO thin films with different thickness on STO and MgO substrates. Thermal evolution of the magnetisation behaves similarly to the target in thick films (same T_C) on MgO and on STO, but thin films exhibit faster drop and reduced T_C.

For the same film thickness, those films deposited on STO exhibit faster drop of the magnetisation and reduced T_C when compared with those deposited on MgO. Consequently, as all the films were deposited using the same procedure, we conclude that the origin of the reduced T_C in these thin films is the substrate-induced strain originated by the film-substrate lattice mismatch.

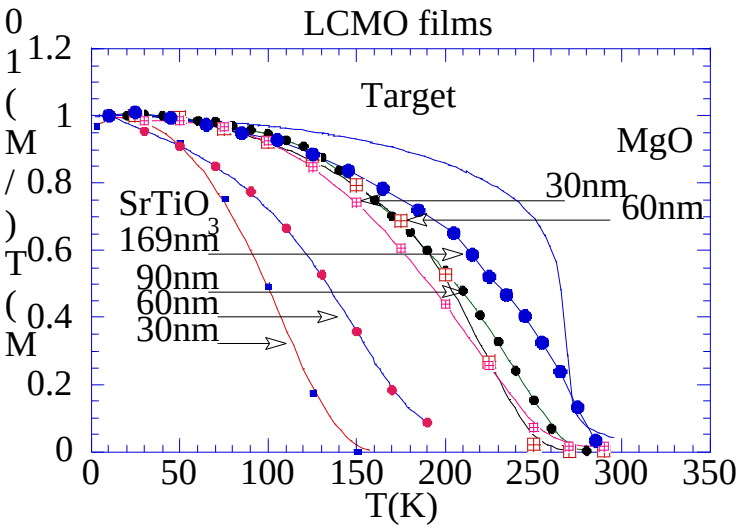

Fig. 4-9 *Evolution of normalised spontaneous magnetisation with temperature for several film thickness and different substrates.*

From the experimental point of view, the exact value of the saturation magnetisation is often difficult to extract in thin films by standard VSM or SQUID techniques because of the errors associated to the film volume determination. In addition, difficulties in measuring the magnetisation in the PM phase do not allow to use the Curie-Weiss law to determine T_C, hence we define T_C as the temperature of the maximum slope in the M(T) curves.

In the following, we will discuss about the effect of strain induced by epitaxial growth on the transport properties of the films.

From transport measurements performed at zero applied magnetic field the residual conductivity has been extracted and is shown in Fig. 4-10. The residual conductivity is highly reduced in fully strained films while for films thicker than the critical thickness, residual conductivity displays a significant augmentation. The reduction of the conductivity for very thin films has been often explained based on the existence of an electrical dead layer due to structural distortions induced at the substrate-film interface.

It has been shown that FM exchange interactions are reduced in films thinner than the critical thickness, hence, the electrical transport should be also reduced in the DE scenario. This means that we would expect the existence of a less conducting (dead) electrical layer which thickness depends on the substrate-film lattice mismatch. In agreement with these ideas, some authors [131] have experimentally deduced a dead electric layer thickness of about 30-50 Å in $La_{2/3}Sr_{1/3}MnO_3$ films on $NdGaO_3$ and $LaAlO_3$.

The electrical dead layer thickness for films on $SrTiO_3$ which has larger mismatch is expected to be larger. Experimentally, from the linear extrapolation of our residual conductivity measurements we found a electrical dead layer in the LCMO/STO system to be about some few tenths of nm (≈60nm). Ziese et al in unpublished data estimated the electrical dead layer for the LCMO/STO system to be 10nm which is smaller than the value we obtained.

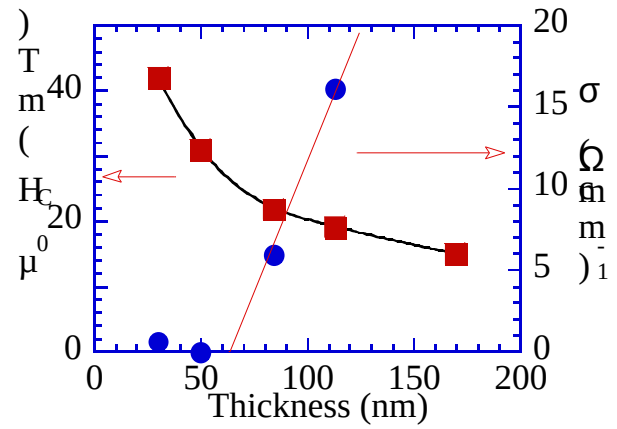

Fig. 4-10 *Measured coercive field at 10K and residual conductivity vs film thickness.*

One striking point is the consideration of the fully strained film thickness as electrically dead. In this work, we have found the relation between the modification of the magnetic and electrical properties and the epitaxial strain. Films thinner than the critical thickness for strain release display lower T_C and in manganites that gives rise to larger residual resistivity and CMR. Hence, it results straightforward to identify the dead layer to the fully strained thickness of the film and to understand its origin on the basis of the DE theory. The differences in the dead layer thickness between different authors can be understood as being originated by the different film growth process and annealing which lead to the partial relaxation of the strain and thus to a reduction of the critical thickness.

The above argument agrees with the analysis of the isothermal M(H) measurements performed at 10K, with the applied magnetic field in the film plane, in order to obtain the variation of the coercive field with the film thickness (Fig. 4-10). The coercive field is reduced when the film thickness increases but no major feature indicating a degradation of the film is observed below the critical thickness. The increase of H_C with the decrease of the film thickness can be explained considering that the nucleation of antiparallel domains and/or pinning at the surface is more important in thin films.

In the following we focus on the variation of the CMR, determined at T_C from magnetotransport measurements, with the film thickness.

In polycrystalline samples, the dependence of the CMR at T_C has been usually related with value of the resistance at T_C. Due to the insulating behaviour of the manganite samples in the PM state, when the PM-FM transition takes place at low temperatures, the resistance at the transition temperature is high and thus under an applied magnetic field the change in the resistance at T_C (CMR) is very large. Consequently, samples with lower T_C exhibit larger values of the CMR and a exponential dependence is observed between MR=ΔR/R (5-12T) and T_C [132]. We have found a similar relation between the MR and the T_C in our series of LCMO films on STO substrate. The exponent extracted from the fit of epitaxially strained films is about –0.037 %MR/ K is similar to the value obtained in polycrystalline samples as shown in Fig. 4-11. Nevertheless, the CMR in our films for a certain value of T_C is about two orders of magnitude larger than in powder samples.

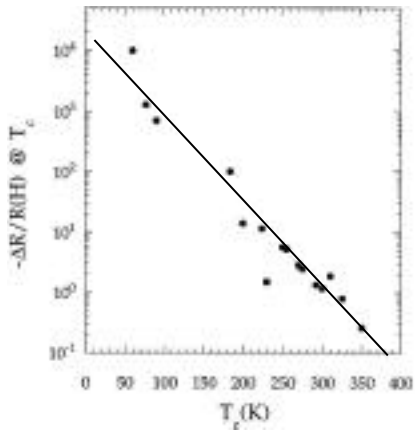

Fig. 4-11 *Graph extracted from [132] displaying the exponential behaviour of the ΔR/R(H) at T_C.*

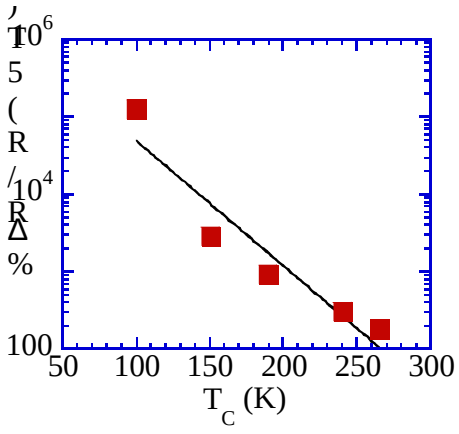

Fig. 4-12 *ΔR/R(5T) at T_C vs T_C in LCMO films on STO being epitaxial strain the tuning mechanism of T_C.*

In conclusion, from magnetotransport measurements we conclude that it is likely the so called dead layer corresponds to the strained film thickness which is highly resistive due to the lower intensity of the FM exchange interaction (DE).

The highly resistive dead layer has been shown to correspond to the fully strained film thickness (≈60±10nm) and its value depends on the film growth conditions and thermal treatments.

This arguments agree with the fact that the resistivity of films thinner than the critical thickness are still measurable.

In the following, we will discuss a possible origin of the change in the magnetic coupling due to epitaxial strain based on the modification of the Mn-O-Mn bonds.

Discussion

In the above section, we have described the structural changes associated to the growth of thin films of LCMO on mismatched STO and MgO substrates. We concluded that thin LCMO films on STO exhibited a shortened out of plane cell parameter and an expanded *a* and *b* cell parameters. In order to understand the effect of the reduction or expansion of the cell parameters on the magnetic properties, we will firstly introduce the effect of hydrostatic and of internal chemical pressure on the properties of bulk manganite and parent compounds.

Experimental observations in the series of compounds $Ln_{2/3}(Ca,Sr)_{1/3}MnO_3$, at constant doping level, where the substitution of the A-cation by another cation with different size produces internal chemical pressure, demonstrate that the mean <Mn-O> (d_{Mn-O}= 1.96 Å) does not change meaningfully through the series [8, 44, 48, 118, 120].On the other hand, in manganites as well as in nickel perovskites, relevant change in the d_{Mn-O} have been observed under applied hydrostatic pressure using neutron diffraction [120, 121].

The main factor for the change in T_C in samples due to substitution of the lanthanide (internal pressure) has been attributed to changes in the Mn-O-Mn bond angle, while in samples under external applied pressure the changes in d_{Mn-O} are larger and constitute the main factor determining the change of T_C.

The effect of an applied hydrostatic pressure onto the manganite perovskite structure is to make a more compact structure. The application of hydrostatic pressure bends the <Mn-O-Mn> angle and decreases d_{Mn-O}. This latter effect is the dominant one and is at the origin of the enhancement of the FM interactions (and T_C) because of enhanced hopping integrals (DE mechanism).

In the DE model, the Mn-O-Mn bond angle is strongly related to the electron transfer integral between neighbouring Mn ions. The tight-binding band model used by De Gennes [15] finds the following expression for the transfer integral between neighbouring Mn-sites:

$$t_{ij} \approx b_{ij} \cos\left(\frac{\beta_{ij}}{2}\right) \qquad \textbf{Eq. 4-2}$$

where b_{ij} characterises the Mn-O-Mn bond, and β_{ij} is the angle between neighbouring Mn moments. The parameter b_{ij} has been expressed as:

$$b_{ij} \approx \varepsilon_\sigma \lambda_\sigma^2 \cos\phi \qquad \textbf{Eq. 4-3}$$

where ε_σ is the one-electron energy, λ_σ is the covalent-mixing parameter of the e_g orbitals of the Mn ion and the σ bonding p orbitals of the oxygen. And $\theta=(180°-\varphi)$ is the Mn-O-Mn bond angle.

The bandwidth is related to the transfer integral by:

$$w_\sigma \quad 2zt_{ij} \qquad \textbf{Eq. 4-4}$$

where *z* is the coordination number. Hence, a modification of the Mn-O-Mn angle produces a change in the Mn_{eg}-$O_{2p\sigma}$-Mn_{eg} overlap. Thus, the bending of the Mn-O-Mn bond angle or an expansion of the Mn-O distance, reduces the transfer integral and consequently the bandwidth. In addition, in [44], a direct relationship between the variation of T_C and of the bandwidth has been reported.

In the following, we will discuss the effect of biaxial strain and the distortions associated to it in the magnetic interactions. We based our discussion in two hypotheses.

Hypothesis I: Tetragonal distortion induces changes in the tilting of the oxygen octahedra (d_{Mn-O} constant)

We will firstly evaluate if the effect of biaxial strain can be only associated to a change on the Mn-O-Mn angle as in the case of internal pressure experiments.

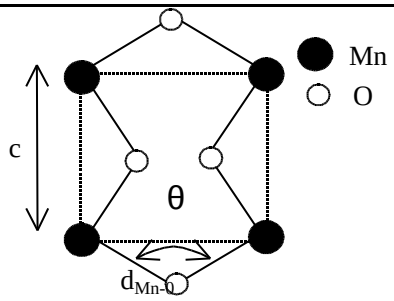

Fig. 4-13 *Schematic representation of a distorted plane in perovskite structure*

We have estimated the values of the Mn-O-Mn angles from the cell parameters of our films using a simple geometrical model (Fig. 4-13). In this model, we assume that d_{Mn-O} remains constant in our series of films. Hence, if the lattice parameter is smaller than $2*d_{Mn-O}$ =3.92 Å, the main effect of a lattice parameter reduction is a decrease of the Mn-O-Mn angle. For larger lattice parameters, there should exist is a stretching of the Mn-O bond. Consequently, we calculate the Mn-O-Mn angle as schematically shown in Fig. 4-13 by:

$$\theta = 2\arcsin\left(\frac{c}{2\,d_{Mn-O}}\right) \qquad \textbf{Eq. 4-5}$$

Using the measured pseudo-cubic *a* and *c* cell parameters, we deduce the in plane and out of plane Mn-O-Mn angles in the above approximation. The calculated in plane and out of plane Mn-O-Mn angles as well as the mean <Mn-O-Mn> obtained are shown in Fig. 4-14. In the same figure, the

evolution of T_C with the film thickness is presented. It can be observed that the calculated mean <Mn-O-Mn> does not meaningfully change with film thickness. Besides, the value of the in plane Mn-O-Mn, obtained from our geometrical model, increases when reducing the film thickness in contrast to the out of plane Mn-O-Mn angle which is highly reduced in the thinner films.

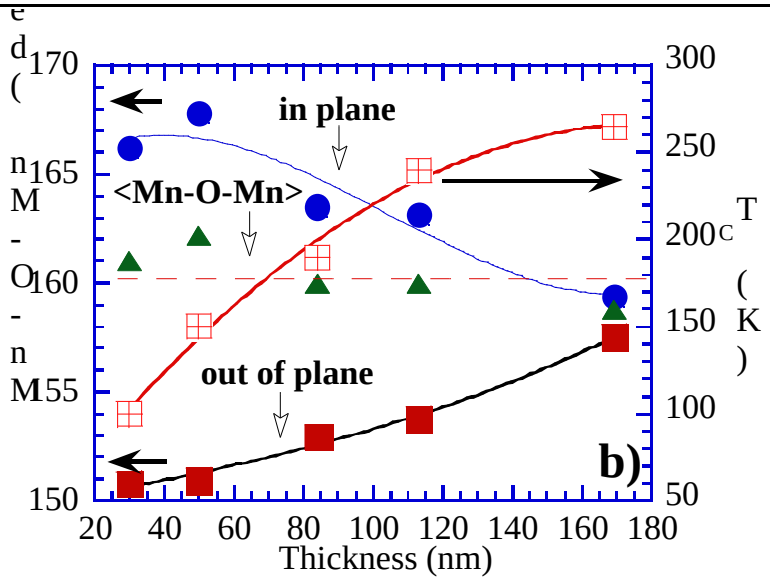

Fig. 4-14 *Measured T_C and estimated values of the in plane, out of plane and means values of the Mn-O-Mn angles of LCMO films on STO substrates (for fixed d_{Mn-O})*

Considering that FM-interactions are purely governed by the DE, we conclude that, in this approximation of constant d_{Mn-O} bond distance, the reduction of T_C in fully strained films can only be explained if the out of plane Mn-O-Mn angle tunes T_C.

The bond angle narrowing diminishes the one-electron bandwidth, *w*, because the effective d electron transfer interaction between neighbouring Mn ions is done via the oxygen 2p states. Considering the hybridisation of the 3d e_g states with the $2p_\sigma$ states in the strong ligand field approximation for a very small deviation of the cubic perovskite ($GdFeO_3$ which has quasi-non tilted FeO_6 octahedra slightly tilted), the p-d transfer interaction is scaled, in first approximation, as t^0_{pd} cos(Mn-O-Mn), where t^0_{pd} is the transfer integral for a cubic perovskite [133]. So the transfer integral d-p-d for the e_g electron should be proportional to the bandwidth and to the square of the p-d transfer integral: $w \quad t_{d\text{-}p\text{-}d} \quad (t^0_{pd} \cos(\text{Mn-O-Mn}))^2$. So, the electron bandwidth is expected to display a squared relation with the cosine of the bonding angle.

The calculated Mn-O-Mn out of plane bonding angle as a function of the film thickness for films deposited on MgO and STO as well as the measured T_C are shown in Fig. 4-15. A good agreement between the Mn-O-Mn out of plane angle and T_C is observed.

In conclusion, considering our geometrical model and assuming that d_{Mn-O} are constant under biaxial strain, we deduced the value of the in plane and out of plane Mn-O-Mn bonding angles. The fact that the mean Mn-O-Mn angle does not meaningfully change with the biaxial strain induced made us assume that the narrowest bond angle should govern the weakening of the magnetic interaction and the reduction of T_C.

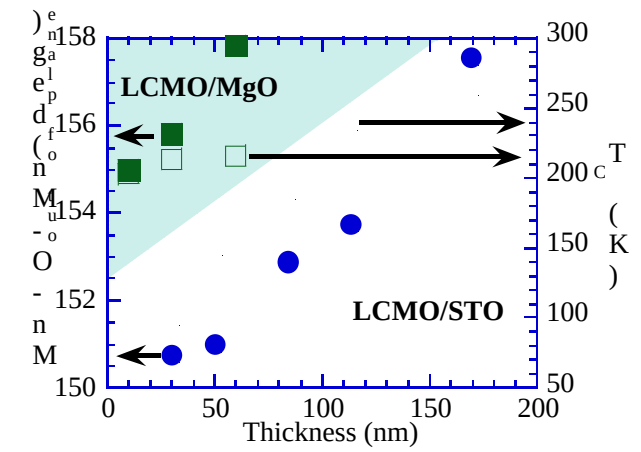

Fig. 4-15 *Dependence of the out of plane Mn-O-Mn angle and T_C with film thickness for LCMO films deposited on STO and MgO.*

The estimated effect of the biaxial strain in the system is to reduce the transfer integral in one direction (*z*-direction) but to increase it in the other two directions (*ab* plane). Hence, in this hypothesis, considering that manganites behave as a Heisenberg ferromagnet, we would expect an enhancement of the FM interactions and thus an increase of T_C and of the metallicity .

Our geometrical model assumed no change on d_{Mn-O} and the main reason for such assumption was found in experimental observations on polycrystalline samples under internal pressure. However, in samples under hydrostatic pressure the change in d_{Mn-O} seems to be the key parameter.

Hypothesis II: Tetragonal distortion induces anisotropic changes in the Mn-O distances in the octahedra (Mn-O-Mn angle constant)

Based in Fig. 4-13 and Eq. 4-5, we can deduce the direct relationship between the change in lattice parameter and d_{Mn-O} :

$$d_{Mn-O} = \frac{c}{2\sin\left(\frac{\theta}{2}\right)} \qquad \textbf{Eq. 4-6}$$

Assuming θ to be constant, the changes in the cell parameters reflect the changes in the Mn-O distances and thus in the Mn (e_g)-O(2p) orbital overlapping. In Eq. 4-2 such overlapping is characterised by λ_σ and hence the transfer integral and the magnetic interaction depends quadratically on this parameter.

From the inspection of the measured cell parameters shown in Fig. 4-3 , we conclude that in this approximation, the in plane Mn-O distance gets larger under biaxial strain, weakening the FM

interactions in the plane. In the out of plane direction, the DE FM interactions should be enhanced due to the reduction of the Mn-O distance in this direction (Fig. 4-16).

Consequently, assuming the biaxial strain to affect mainly the d_{Mn-O}, we obtain that the transfer integral is reduced in two directions (*ab* plane), and is enhanced in only one direction. Hence, in this case, we would expect the system to become less metallic, to have a reduced bandwidth and thus to present a lower T_C as observed experimentally.

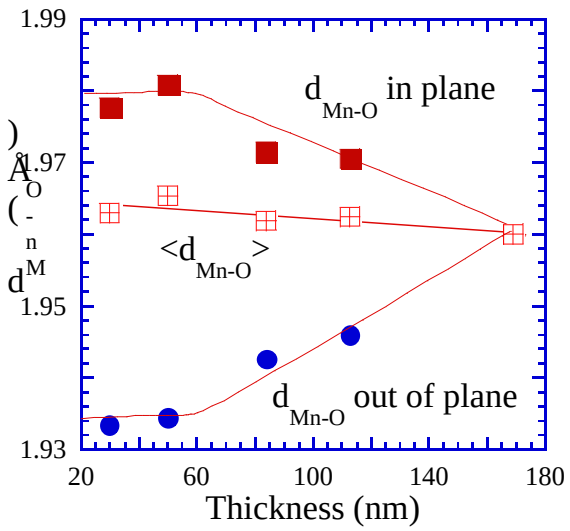

Fig. 4-16 *Calculated Mn-O distances considering Mn-O-Mn angle constant.*

In conclusion, biaxial strain induced by the substrate in our films has been experimentally found to produce larger changes in the *c* parameter than the in plane cell parameters (Fig. 4-7). The tilting of the octahedra in the [001] direction in non strained perovskite is very close to the in plane tilting as extracted from [134](<Mn-O-Mn>(1) = 159.5° <Mn-O-Mn>(2)=160.7°). Hence, even if the metallicity is more favoured in the *c* direction due to a Mn-O bond distance reduction in fully strained films, in the two other directions, *ab* plane, the metallicity is reduced due to the stretching of the bonds (Fig. 4-16). Consequently, a reduction of the FM coupling strength would be expected in the strained films in agreement with the observed magnetic behaviour. However, further measurements compatible with thin film samples, as EXAFS are required to check the validity of our model.

Hence, the results agree with the conclusions extracted from theoretical studies performed by Millis et al.[122]. The authors assumed that biaxial distortion increases the Jahn-Teller splitting (because Jahn-Teller splitting of the E levels is directly proportional to the distortion of the octahedra [135]), and hence the tendency of the electrons to become localised. In this sense, the authors deduced the existence of a relation between T_C and the biaxial strain ε^* through the Δ parameter defined as the e_g level splitting in the Jahn-Teller distortion:

$$\frac{T_C(\Delta) - T_C(0)}{T_C(0)} = \frac{0.5}{T_C(0)} \partial^2 T_C / \partial \Delta^2 \qquad \textbf{Eq. 4-7}$$

The authors approximate the value of $\partial^2 T_C / \partial \Delta^2 \approx 0.4t$, hence meaning that there exist a linear relationship between T_C and the transfer integral *t*. However, the relation between the anisotropic biaxial strain ε^* and T_C which are the only direct measurable parameters was lacking. We have calculated the biaxial strain ε^* for all the films and we have found a quadratic relation between T_C and ε^* (Fig. 4-17). Once we know the experimental relation between T_C and ε^*, determining theoretically the relation between the e_g level splitting , Δ, and ε^* , one can find if the change in T_C due to biaxial strain can only be attributed to level splitting or not.

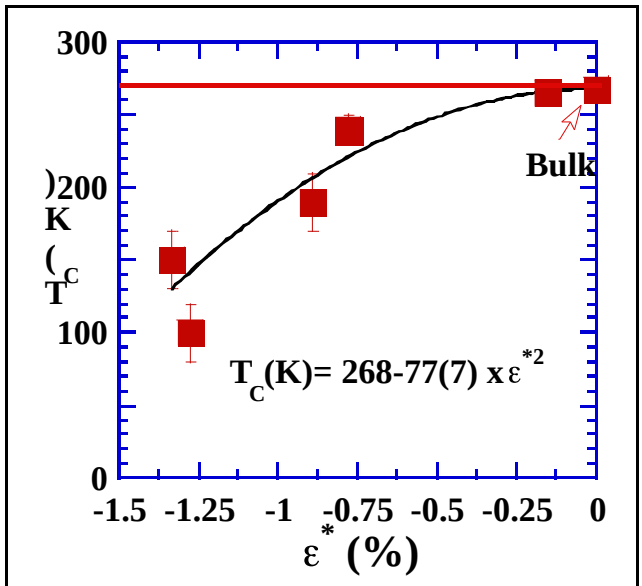

Fig. 4-17 *Experimental relation between the biaxial distortion in epitaxially strained LCMO films on STO and T_C*

Comparison with the effect of hydrostatic pressure

In the following, we will compare the effect of biaxial strain to the effect of hydrostatic pressure on the change of T_C . The application of a biaxial strain changes T_C by -125K/% biaxial strain (considering $T_C(\varepsilon^*)$ in first approximation to be linear). However, in order to compare it with the effect of hydrostatic pressure on $La_{2/3}Ca_{1/3}MnO_3$ bulk samples (2.2K/kbar) extracted from [46, 119], the relation between the change of the cell parameter with the applied external pressure is needed. Considering the values of the Mn-O-Mn angle and Mn-O compressibility extracted from [120] ($k_p^w = \frac{1}{\cos(w)} \frac{\partial \cos(w)}{\partial P} = 2.1 10^{-4} kbar^{-1}$ and ω=0.5(π-<Mn-O-Mn>), $k_p^{d_{Mn-O}} = \frac{1}{\langle Mn-O \rangle} \frac{\partial \langle Mn-O \rangle}{\partial P} = -2.32\ 10^{-3} kbar^{-1}$) and considering Eq. 4-6 we deduce the change of the lattice parameters under an applied external pressure as:

$$\frac{\Delta c}{c} kbar^{-1} = \frac{2}{c} < d_{Mn-O} > k_p^{d_{Mn-O}} \sin\left(\frac{\theta}{2}\right) + \frac{< d_{Mn-O} >}{c} \cos\left(\frac{\theta}{2}\right) \frac{2 k_p^{\omega}}{\tan(\omega)} \qquad \textbf{Eq. 4-8}$$

Using the values for d_{Mn-O} =1.962Å and <θ>=159.9° and *c*≈3.862Å extracted from [134], we found a variation of the lattice parameter of about –2.1 10^{-1} ε(%)/kbar. The change in the unit cell parameter due to the application of hydrostatic pressure is mainly due to the change of the <Mn-O> bond distance. That means that in order to obtain 1% of lattice parameter change using hydrostatic

pressure, 470 kbar would be needed. The difference between the effect of hydrostatic pressure and biaxial strain is that the latter conserves the unit cell volume while the former changes the volume of the unit cell.

The application of hydrostatic pressure modifies the value of T_C because of the enhancement of the FM interactions in the three directions of the Mn-O bonds. Hence, a change of 1% in lattice parameter induced by hydrostatic external pressure would induce an enhancement of T_C of about 10K. This result contrast with the changes in T_C obtained under 1% of biaxial strain using epitaxial growth, which produces a reduction of T_C of about -121K.

Therefore, while hydrostatic pressure reduces the d_{Mn-O} in the three directions of the Mn-O bonds producing an enhancement of the FM interactions, biaxial strain induced by epitaxial growth of LCMO on STO is likely to produce a reduction of the out of plane Mn-O bond length but increases the bond lengths in the *ab* plane reducing the DE transfer integral and thus T_C.

In the following section, we will study the magnetic anisotropy induced in the films of LCMO on STO due to the tetragonal distortion caused by the strain induced through epitaxial growth on mismatched STO substrate.

4.3 Magnetic Anisotropy induced by epitaxial strain

Magnetic loops measured in the perpendicular geometry show that the [001] axis is a hard axis. The magnetic anisotropy is thickness dependent as shown in (Fig. 4-18). Lattice distortion due to epitaxial strain in thin LCMO films on STO could be at the origin of the out of plane magnetic anisotropy.

From the inspection of the M(H) curves performed at 10K (Fig. 4-18) it can be detected the existence of a small remanence. The existence of small remanence in magnetic loops perpendicular to the plane of the film can be explained to be originated by a slight misalignment of the sample respect to the applied field in our experimental set-up because no evidence of a second crystallographic texture has been observed which can be at the origin of a second order anisotropy.

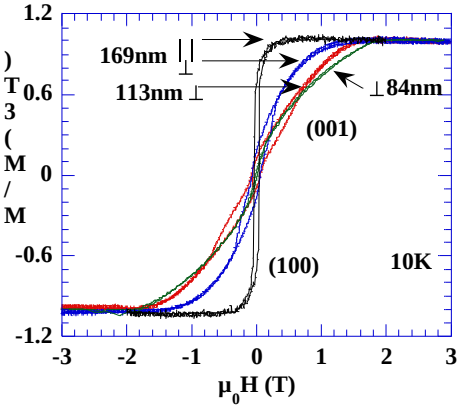

Fig. 4-18 *Hysteresis loops measured at 10K in parallel and perpendicular geometry on films with thickness ranging between 84 to 170nm*

In a sample, the magnetic moment tends to align preferably in certain directions (easy directions) because of non-spherical environment. In a thin film,

the main effect is the shape anisotropy, which is the result of the minimisation of the magnetostatic energy. In order to evaluate if biaxial strain could be the origin of the out of plane magnetic anisotropy observed we will firstly evaluate the different terms contributing to the total magnetic energy in our sample.

The total (magnetic-elastic) energy of a film can be expressed as:

$$E = E_0 + E_a + E_{me} + E_{el} - \vec{M}\ \vec{H} \qquad \textbf{Eq. 4-9}$$

where E_0 is the magnetic energy independent of the magnetisation direction, E_a is the magnetocrystalline energy, E_{me} is the magnetoelastic energy, E_{el} is the elastic energy and the last term corresponds to the magnetostatic energy being $\vec{H} = \vec{H}_a + \vec{H}_D$ (a= applied and D= demagnetising).

For tetragonal symmetry, the magnetic anisotropy energy can be expressed in the following way:

$$E_a = K_1 m_z^2 + K_2 m_z^4 + K_3 m_x^2 m_y^2 \qquad \textbf{Eq. 4-10}$$

where $m_{x,y,z}$ are the director cosines of the magnetisation vector with respect the crystal axis. The energy differences measured in different directions give the values of the anisotropy constants: $E_{[001]} - E_{[100]} = K_1 + K_2$, while $E_{[110]} - E_{[100]} = K_3/4$.Cubic symmetry implies $K_1 = K_3 = -K_2$.

The anisotropy field found in strained films is about 1T for thinner films and could have several contributions: the intrinsic cubic magnetocrystalline anisotropy, the strain induced magnetoelastic anisotropy and the anisotropy induced by magnetostrictive strains appearing when the magnetisation changes direction. We have neglected the surface anisotropy because the thinnest film (30nm) cannot be considered thin enough to present important, relative to the volume term, surface anisotropy. However if such source of anisotropy had to be considered an term analogous to the anisotropy energy but inversely proportional to the film thickness has to be considered [136] [137, 138]. On the other hand, contributions from intrinsic magnetocrystalline bulk anisotropy are negligible compared to magnetoelastic coupling due to epitaxial strain because in thick films (and single crystals $K_1 \approx 3610^{-3}$) we do not observe the existence of magnetic anisotropy in the out of plane direction.

In the following, the equations concerning the expression of the different contributions to the total magnetic energy will be described. These equations have been extracted from [139, 140].

The magnetoelastic energy can be expressed in a cubic symmetry as:

$$E_{me} = b_0\left(\varepsilon_{xx} + \varepsilon_{yy} + \varepsilon_{zz}\right) + b_1\left(m_x^2\varepsilon_{xx} + m_y^2\varepsilon_{yy} + m_z^2\varepsilon_{zz}\right) + \\ + b_2\left(m_x m_y \varepsilon_{xy} + m_y m_z \varepsilon_{yz} + m_z m_x \varepsilon_{zx}\right) \qquad \textbf{Eq. 4-11}$$

While the elastic energy can be expressed as:

$$E_{el} = \frac{1}{2}c_{11}\left(\varepsilon_{xx}^2 + \varepsilon_{yy}^2 + \varepsilon_{zz}^2\right) + c_{12}\left(\varepsilon_{yy}\varepsilon_{zz} + \varepsilon_{zz}\varepsilon_{xx} + \varepsilon_{xx}\varepsilon_{yy}\right) + \frac{1}{2}c_{44}\left(\varepsilon_{xy}^2 + \varepsilon_{yz}^2 + \varepsilon_{zx}^2\right) \quad \textbf{Eq. 4-12}$$

Magnetostriction, Δl/l, in cubic symmetry can be expressed as a function of the two lowest order terms as:

$$\frac{\Delta l}{l} = \sum_{i \geq j} \varepsilon_{ij}^{eq}\beta_i\beta_j \approx \lambda^{\alpha} + \frac{3}{2}\lambda_{100}\left(m_x^2\beta_x^2 + m_y^2\beta_y^2 + m_z^2\beta_z^2 - \frac{1}{3}\right) + 3\lambda_{111}\left(m_x m_y \beta_x\beta_y + m_y m_z \beta_y\beta_z + m_z m_x \beta_z\beta_x\right) \quad \textbf{Eq. 4-13}$$

where ε_{ij}^{eq} are the equilibrium strains determined from the minimisation of the total magnetic energy with respect to the strains. m_i the direction cosines of the magnetisation direction with respect to the crystal axes and β_i are the direction cosines of the deformation measurement direction with respect to the crystal axes.

Supposing that the tetragonal distortion measured at room temperature remains when cooling down towards the magnetic transition temperature as observed in bulk samples[10], in the FM state $\varepsilon_{xx}=\varepsilon_{yy}$ and $\varepsilon_{xy}=0$. The equilibrium strains are determined from the minimisation of the energy E and from $\partial E/\partial\varepsilon_{zz} = 0$ and $\partial E/\partial\varepsilon_{xz} = 0$ equation we obtain:

$$\varepsilon_{zz}^{eq} = -b_0/c_{11} - b_1 m_z^2/c_{11} - c_{12}\,2\varepsilon_{xx}/c_{11} \quad \textbf{Eq. 4-14}$$

and

$$\varepsilon_{ij}^{eq} = -b_2 m_i m_j / c_{44} \quad \textbf{Eq. 4-15}$$

for ij=xz and ij=yz.

Introducing the above values in Eq. 4-13 we deduce the values of the magnetostriction constants in a cubic system [141]:

$$\lambda_{001} = \frac{-2b_1}{3c_{11}} \quad in \quad thin \quad films$$
$$\lambda_{111} = \frac{-b_2}{3c_{44}} \quad \textbf{Eq. 4-16}$$

When substituting the equilibrium strains in the total energy and identifying the coefficient of m_z^2 to K_1 we obtain (if considering the intrinsic cubic magnetocrystalline anisotropy and the magnetostrictive terms to be negligible):

$$K_1 = b_1\left(\varepsilon_{zz}^{eq} - \varepsilon_{xx}\right) \quad \textbf{Eq. 4-17}$$

Moreover, $\sigma_{ij} = c_{ijkl}\varepsilon_{kl}$, and thus $\sigma_{xx} = c_{11}\varepsilon_{xx} + c_{12}\varepsilon_{yy} \approx 2c_{11}\varepsilon_{xx}$ if we consider $\varepsilon_{xx}=\varepsilon_{yy}$ and $c_{11}\approx c_{12}$. So, K_1 can also be expressed as a function of the magnetostriction constant λ_{001} as:

$$K_1 = b_1\left(\varepsilon_{zz}^{eq} - \varepsilon_{xx}\right) \approx b_1\left(\frac{c_{12}}{c_{11}} - 1\right)\varepsilon_{xx} \approx -2b_1\varepsilon_{xx} = 3\lambda_{001}\sigma_{xx}/2 \qquad \textbf{Eq. 4-18}$$

In the perpendicular geometry, the saturation field (H_S) can be related to the uniaxial anisotropy ($K_u \approx K_1$ in first order approximation). The relationship between the saturation field and the anisotropy constant can be obtained from the minimisation of the sum of the magnetostatic energy ($E_m=(\mu_0/2)NM^2_S\sin(\theta)$), the anisotropy energy ($E_A=K_1\sin^2(\theta)$) and the term which couples with the applied magnetic field ($E_B=-M_S B_0\sin(\theta)$) respect to the angle (θ) of the magnetisation respect to the crystallographic axis which permits to obtain a value of the equilibrium angle of the magnetic moments (which tend to align to the direction of the applied field). The equilibrium angle is related to the magnetisation by $M=M_s\sin(\theta)$, and taking into account that M=Ms when $H=H_s$ in the perpendicular geometry, the following relation can be obtained:

$$H_S = NM_S + 2K_u/M_S \qquad \textbf{Eq. 4-19}$$

where N is de demagnetising factor which in perpendicular geometry is equal to the unity.

In order to determine experimental uniaxial anisotropies from H_s, we used the theoretical M_S value (the experimental uncertainties associated to the thickness of the films and surface, precluded to obtain experimental M_s accurately). $M_S \approx 0.74$T for a doping level of x=1/3.

According to Fig. 4-19 the uniaxial anisotropy constant for fully strained films is about $K_u=2\ 10^5$J/m^3 and when the biaxial strain is released, the value of the anisotropy constant decreases rapidly in agreement with the fact that the existence of magnetic anisotropy is due to magnetoelastic effects. The obtained value is similar to the anisotropy constant reported in $La_{0.8}Ca_{0.2}MnO_3$ on STO substrates ($1.8\ 10^5$ J/m^3) [142].

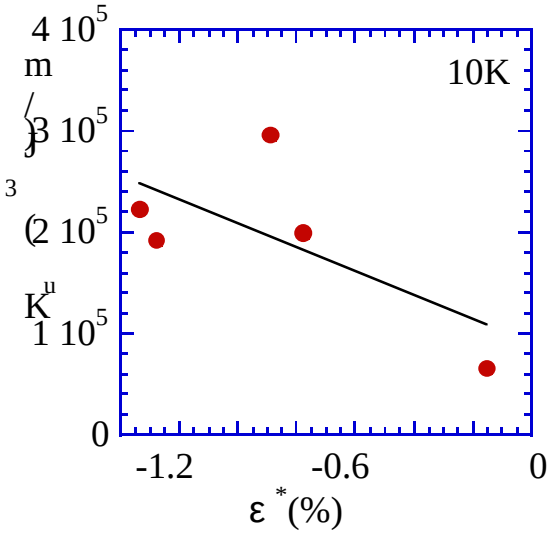

Fig. 4-19 *Relation between the anisotropy constant and the biaxial strain in epitaxially strained LCMO films on $SrTiO_3$ substrates.*

We have found a direct linear relation between the anisotropic distortion and the magnetic anisotropy constant for films in the thickness range between 60 to 170nm (Fig. 4-19). The slope is $1.7\ 10^5$ J/m^3 per % of biaxial strain.

For films thinner than 60nm we observed a saturation of the anisotropy constant. This fact can be explained if we consider that films thinner than 60nm are fully strained thus no evolution of the anisotropy constant is expected when reducing the film thickness (in the film thickness range where the surface anisotropy can be neglected).

In the above estimations, we have assumed that the films were homogeneous magnetically and structurally. However in section 4.1 we observed that films LCMO films on STO substrates thicker than 60nm present larger Bragg peaks, thus meaning the existence of cell parameter relaxation through the film thickness. From the magnetic point of view, in the above estimations we have not take into account the possible diminution of the FM interactions or their disappearance at the interfaces as has been predicted theoretically [111]. So if non FM interactions exist at the free surface or interface between the film and substrate, they will diminish the value of M_{sat} and will contribute more as thinner are the films. Weakened FM interactions are expected also to exist due to lattice distortion as well as to the broken symmetry at the surface.

In the following, we will try to estimate the value of the magnetostriction constant λ_{001} from our experimental measurements. Considering the value of K_1 we found, we have determined the values of the magnetostriction constant λ_{001} using the values of c_{11}, extracted from the literature, measured on a single crystal of the parent compound $La_{0.83}Sr_{0.17}MnO_3$ (c_{11}=206GPa=2.06 10^{12} erg/cm^3) [143]. For fully strained films we deduced a value of $\lambda_{001}=2.810^{-5}$. This value is similar to the value given in [142] for a 25 nm thick $La_{0.8}Ca_{0.2}MnO_3$ on STO substrates by PLD (λ_{001}=3 10^{-5}) and to the calculated value obtained from first principles (λ_{001}=2.1 10^{-5})[136]. However, in [144] for a 58nm thick LCMO film on STO deposited by MBE the experimental value is rather large (λ_{001}= 7 10^{-5}).

The magnetoelastic coupling constant b_1 can also be obtained from the value of K_u and in our films the obtained value is about -8.9 10^6 J/m^3 and is also comparable to the values given by O'Donnell –6.7 10^6 J/m^3 (Fig. 4-20).

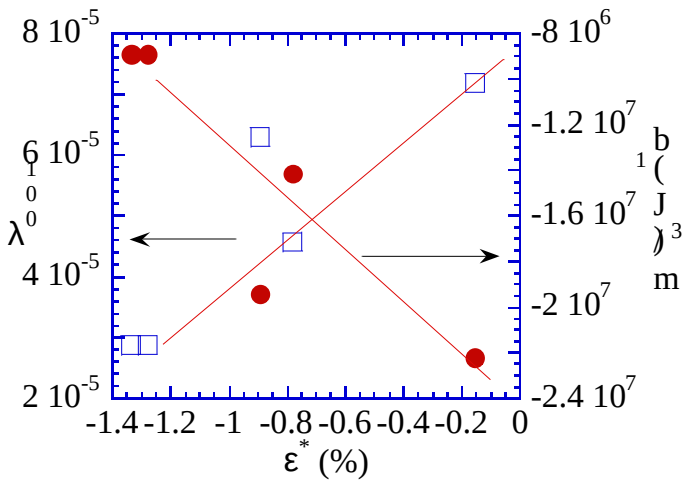

Fig. 4-20 *Magnetostriction and magnetoelastic constants obtained for epitaxially strained films of LCMO on STO.*

In conclusion, in fully strained films the out of plane cell parameter is reduced compared to the in plane cell parameters. In the tetragonal crystal an extra splitting of the e_g orbitals and thus increasing the tendency of the

electrons to localise. From the magnetic point of view the apparition of anisotropy can be explained by magnetoelastic effects associated to the lattice distortions due to the epitaxial strain.

4.4 Conclusions

In this chapter, we have studied the effect of epitaxial strain on the magnetic and transport properties of $La_{2/3}Ca_{1/3}MnO_3$ thin films.

We have grown a series of LCMO films with different thickness on $SrTiO_3$ (001) substrates and a detailed structural characterisation has been carried out. We have identified the existence of a critical film thickness for the onset of structural relaxation process of about 60nm (1%biaxial strain).

LCMO films on STO substrates with thickness below the critical value show reduced T_C, large residual resistivity, and large values of the CMR. These features can be explained to be originated by a reduction of the DE interaction in strained films. The origin of the reduction of the DE interaction has been discussed. The most likely effect of biaxial strain seems to be the modification of the d_{Mn-O}. However, further study would be needed to clarify this point.

Magnetic Anisotropy has been observed in strained films. It has been related to magnetoelastic effects associated the lattice distortions due to the epitaxial strain.